analytical chemistry

Article

pubs.acs.org/ac

Controllable Preparation of $CuFeMnO_4$ Nanospheres as a Novel Multifunctional Affinity Probe for Efficient Adsorption and Selective Enrichment of Low-Abundance Peptides and Phosphopeptides

Xing-Yu Long,[†,‡] Zi-Jin Zhang,[†] Jia-Yuan Li,[†] Dong Sheng,[†] and Hong-Zhen Lian*[,†]

[†]State Key Laboratory of Analytical Chemistry for Life Science, Collaborative Innovation Center of Chemistry for Life Sciences, School of Chemistry & Chemical Engineering and Center of Materials Analysis, Nanjing University, Nanjing 210023, China

[‡]Editorial Department of Journal, Guizhou Normal University, Guiyang 550001, China

Supporting Information

ABSTRACT: A facile solvothermal method for the synthesis of multifunctional magnetic $CuFeMnO_4$ nanospheres affinity probe (NSAP) with controllable morphology and size was developed for the first time. The $CuFeMnO_4$ nanospheres combine the brilliant features of Cu^{2+}, Fe^{3+}, and Mn^{2+} ions, so their multifunction performances are embodied by strong coordination to carboxyl and amine groups of peptides (Cu^{2+} and Fe^{3+}), special affinity to phosphate groups of phosphopeptides (Fe^{3+} and Mn^{2+}), and high magnetic responsiveness in a magnetic field. Their potential as an affinity probe was evaluated for highly effective enrichment, rapid magnetic separation of low-abundance peptides (neutral condition), and effective selective capture of phosphopeptides (acid condition) from various complex biosamples. Notably, $CuFeMnO_4$ NSAP was explored for highly selective capture and isolation of phosphopeptides from A549 cells after exposure to ZnO nanoparticles for different times. Consequently, we put forward a new nanospinel ferrite-based protocol here to analyze and identify the phosphoproteins/phosphopeptides involved in cellular signaling pathways in response to exogenous stimulation.

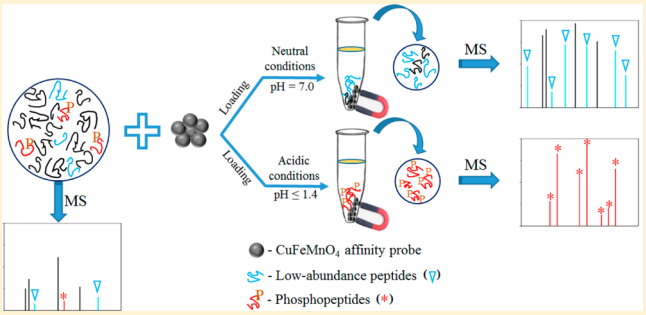

As we all know, protein is an important biomarker of some diseases, such as cancer, Alzheimer's disease (AD), cardiovascular disease, diabetes, Parkinson's, osteogenesis imperfecta, and so on.[1−5] Shotgun proteomics based on mass spectrometric (MS) analysis can globally isolate and identify the expression proteins of tumor cells, and it is often used to screen biomarker proteins of these diseases in high-throughput proteomics research.[6] However, some low-abundance peptides show potential as biomarkers, including post-translational modifications of proteins hydrolysates, such as phosphopeptides and glycopeptides, and they are expressed at extremely low concentrations (less than 1 nM). They often suffer from being lost in direct MS detection from complex biological matrixes due to their low ion intensity as well as the signal suppression effect and interference from other high-abundance peptides and/or contaminations (salts and surfactants).[7] Moreover, as biomarkers, many reported low-abundance biologically active peptides, such as cytokines and hormones, may provide valuable information for pathogenesis, early diagnosis, and treatment of disease.[8,9] Thereby, highly selective enrichment of low-abundance peptides including phosphopeptides and glycopeptides has attracted tremendous attention in proteomics/peptidomics research.[10−15] It is a critical factor to develop novel affinity materials for efficient enrichment and selective extraction of low-abundance peptides.

Recently, on the basis of special enrichment mechanisms, for instance, hydrophobic interaction or coordination for general low-abundance peptides, affinity interaction (electrostatic, coordination, and chelation) for phosphopeptides, and hydrophilic interaction for glycopeptides, numerous innovative nanomaterials have been designed and exploited.[16−18] To date, on the basis of the affinity interaction between metal ions/oxides and functional groups with target peptides, some effectual measures have been implemented and improved by integrating mesoporous[19−21] or 2-dimensional[22,23] structured and magnetized materials[24] to realize the aim of size exclusion or expand the surface area for enlarging binding sites, and easy and fast magnetic separation. In spite of the rapid development of materials science, it is still a huge challenge for applying novel affinity materials to effectively enrich low-abundance peptides, together with selectively capturing and isolating phosphopeptides from the complex biological samples prior to matrix-assisted laser desorption/ionization time-of-flight mass spectrometry (MALDI-TOF MS) analysis.[25] In particular, in view of the merits of excellent monodispersibility, metal ion affinity, and convenient separability, magnetic spinel-type ferrite

Received: June 26, 2017
Accepted: September 4, 2017
Published: September 4, 2017

DOI: 10.1021/acs.analchem.7b02476
Anal. Chem. 2017, 89, 10446−10453

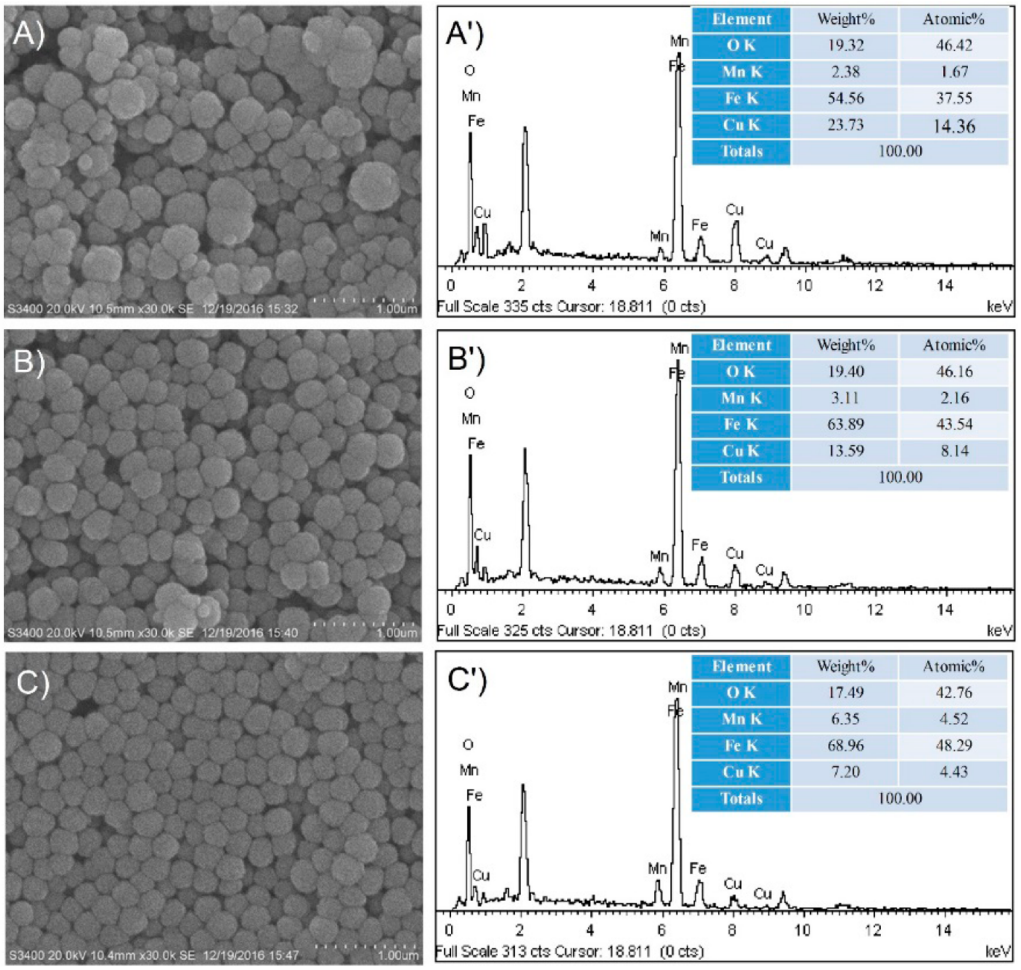

Figure 1. SEM images (left) and EDS spectra (right) of $CuFeMnO_4$-01 (A and A′), $CuFeMnO_4$-02 (B and B′), and $CuFeMnO_4$-03 (C and C′), respectively.

affinity materials have obtained considerable interest in the bioenrichment field.[26]

In this present study, a novel solvothermal method was proposed for the synthesis of magnetic spinel-type $CuFeMnO_4$ nanospheres affinity probe (NSAP). Meanwhile, possible formation mechanisms of the uniform $CuFeMnO_4$ NSAP in a liquid-phase process were elucidated. Very interestingly, selective capture of phosphopeptides and effective enrichment of low-abundance peptides were realized, respectively, under different conditions of loading buffer. For the neutral condition (pH = 7.0), $CuFeMnO_4$ NSAP exhibits strong coordination to carboxyl and amine groups of peptides on the basis of their surface with abundant Cu^{2+} and Fe^{3+} ions. Whereas, for the acid condition (pH $\leq$ 1.4), the NSAP possesses a high binding affinity toward phosphopeptides because Fe^{3+} and Mn^{2+} ions can interact with phosphate moieties of phosphopeptides. Models of tryptic digests of low concentration of BSA (10 nM) and mixture of α- and β-casein (v/v = 1:1), respectively, for low-abundance peptides and phosphopeptides, were chosen for proof-of-principle demonstrations. In addition, $CuFeMnO_4$ NSAP was utilized for selectively extracting and separating phosphopeptides from the lysates of intricate A549 cells treated with ZnO nanoparticles for different time. The change of phosphoproteins expression involved in the cellular signaling pathways in response to the exogenous stimulation was observed.

EXPERIMENTAL SECTION

Chemicals and Materials. Common chemicals and reagents were obtained commercially from various suppliers (see PART 1 in Supporting Information) and used as received without further purification. Nonfat milk was purchased from Jiangsu Province Educational Supermarket. Human saliva and serum samples from a healthy volunteer were provided by Nanjing University and obtained according to the standard clinical procedures. Human lung adenocarcinoma cells (A549 cells) were exposed to 5 mg/L of ZnO nanoparticles and incubated in culture medium for 0, 9, and 24 h in another work in our laboratory. The samples were stored at −80 °C before analysis. Ultrapure water (18.2 MΩ·cm) was prepared with a Milli-Q water purification system (Millipore, Billerica, MA). All of other chemicals were of analytical reagent grade unless otherwise noted.

Synthesis and Characterizations of $CuFeMnO_4$ NSAP. $CuFeMnO_4$ NSAP was prepared by a solvothermal reaction. Briefly, NaAc (3.6 g), $FeCl_3{\cdot}6H_2O$ (1.35 g, 5.0 mmol), $CuCl_2{\cdot}2H_2O$ (2.5−5.0 mmol), and $MnCl_2{\cdot}4H_2O$ (2.5−5.0 mmol) were completely dissolved in ethylene glycol (EG, 40 mL) via ultrasonication for 30 min. The effect of mole ratios of Fe^{3+}/Cu^{2+}/Mn^{2+} at 2:2:1, 2:1:1, and 2:1:2 were investigated on the property of the products (denoted as $CuFeMnO_4$-x (x = 01, 02, 03) NSAP, respectively). The obtained homogeneous mixture solution was transferred into a Teflon-lined stainless-steel

DOI: 10.1021/acs.analchem.7b02476
Anal. Chem. 2017, 89, 10446−10453

autoclave and sealed to heat at 200 °C for 8 h. After the reaction, the grayish products $CuFeMnO_4$-x nanospheres were obtained with the help of a magnet. The products were rinsed with ultrapure water and ethanol several times and dried at 60 °C for stay over. The structural and morphological characterizations of $CuFeMnO_4$ NSAP were conducted as shown in PART 1 in Supporting Information.

Sample Preparation and Peptide Enrichment. The details of preparation process of the tryptic digests of α-/β-casein, BSA, nonfat milk and A549 cells lysates, together with extraction of low-abundance peptides and phosphopeptides were also shown in PART 1 in Supporting Information.

MALDI-TOF MS Analysis. After the extraction of target peptides by $CuFeMnO_4$ or other affinity probes from various samples (see PART 1 in Supporting Information), 0.5 μL of the eluate was deposited on a MALDI plate, and then 0.5 μL of DHB aqueous solution (20 mg/mL, 50% ACN and 1% H_3PO_4) was introduced as a matrix to perform the MALDI-TOF MS analysis in a positive ion reflection mode on a 4800 Proteomics Analyzer (Applied Biosystems, Framingham, CT, U.S.A.) with the Nd:YAG laser at 355 nm, a repetition rate of 200 Hz, and an acceleration voltage of 20 kV. Spectra were obtained by accumulation of 2000−3000 consecutive laser shots. Peptide mass fingerprinting (PMF) data were submitted to MASCOT search engine (http://www.matrixscience.com/) for database search and identification of corresponding peptides employing the following search parameter settings. Database: SwissProt; Enzyme: Trypsin; Maximum of missed cleavages: 1; Taxonomy: *Bos taurus*; Peptide tolerance: ± 1.2 Da; Mass values: MH^+, Monoisotopic.

RESULTS AND DISCUSSION

Synthesis and Characterization of $CuFeMnO_4$ NSAP. Jogalekar and his co-workers first reported the preparation of general $CuFeMnO_4$ spinel in 1967 which was a kind of ternary metal oxide.[27] Afterward, Bergstein[28] described the mechanism of changes of the tetragonal deformation of $CuFeMnO_4$ spinel by oxidation−reduction reactions. $CuFeMnO_4$ nanoparticles have been conventionally prepared by using coprecipitation,[29] direct thermal decomposition,[30] and sol−gel methods[31,32] for solar-absorbing. However, in coprecipitation, it is difficult to control all the metal cations to precipitate from the solution at the same time, which results in composition segregation and low yield. In addition, $CuFeMnO_4$ synthesized via thermal decomposition method or sol−gel process often suffers from uncontrollable particle size, or harsh high-temperature reaction condition, or elaborate annealing procedure. In the present work, the $CuFeMnO_4$ spinel nanospheres with uniform dimension were prepared by a solvothermal process for the first time by the reaction of $FeCl_3{\cdot}6H_2O$, $CuCl_2{\cdot}2H_2O$, $MnCl_2{\cdot}4H_2O$, and EG in the presence of NaAc (as an auxiliary agent). The solvothermal process used here was conducive to the decomposition of $Me(OH)_n$ (Me: metallic ions, n: charges) and the crystallization of $CuFeMnO_4$, which avoided cockamamie synthesis method and low yield, and ensured production of preferably dispersible and less agglomerative as well as controllable particles with good shape. Besides, the sol−gel process or solid reaction to produce $CuFeMnO_4$ nanoparticles usually requires a heat treatment at an elevated temperature (e.g., at 700 °C) for the phase transition from $Me(OH)_n$ to $CuFeMnO_4$.[33] In contrast, the energy consumption and production cost of the proposed solvothermal process could be reduced due to the elimination of the heat treatment, allowing for a sufficient energy-efficient way to synthesize uniform and ultrafine nanoparticles.

The morphology and size, and composition of the $CuFeMnO_4$-x nanospheres affinity probes (NSAP) were examined by SEM and EDS, and TEM, respectively. As shown in Figure 1, the sizes of $CuFeMnO_4$-01 and $CuFeMnO_4$-02 are unevenly distributed (Figure 1A,B). Besides, it is clear that some of the $CuFeMnO_4$-01 particles are aggregative, while $CuFeMnO_4$-03 particles consist of monodisperse and uniform nanospheres (Figure 1C). The results from EDX spectrum showed that these $CuFeMnO_4$-x nanospheres contain O, Fe, Mn, and Cu, and no contamination elements are detected (Figure 1A′−C′). The results of TEM (Figure 2) were in good

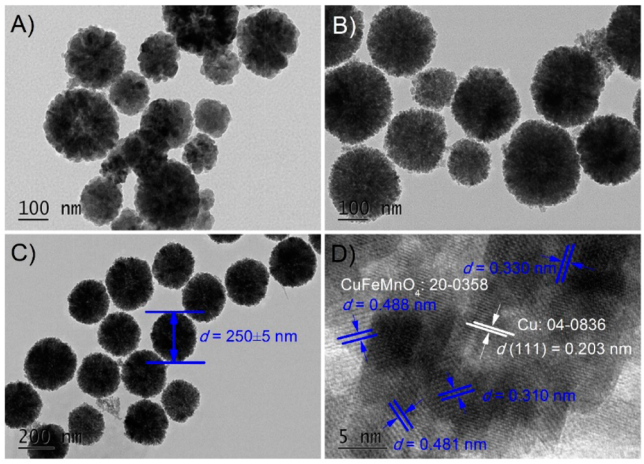

Figure 2. TEM images of $CuFeMnO_4$-01 (A), $CuFeMnO_4$-02 (B), and $CuFeMnO_4$-03 (C), and HRTEM image of $CuFeMnO_4$-03 (D).

agreement with those of SEM, respectively, which indicated the different particle-size distribution of $CuFeMnO_4$-x. The particle size of $CuFeMnO_4$-03 measured from the TEM image is 250 ± 5 nm (Figure 2C). The HRTEM image further confirmed the crystalline structure of $CuFeMnO_4$-03 (Figure 2D). Moreover, $CuFeMnO_4$-03 nanospheres showed well-defined lattice planes with perfect crystallinity (JCPDS No. 20-0358). The crystal lattice fringe with a spacing of 0.203 nm can be assigned to the (111) planes of elemental copper (JCPDS No. 04-0836), which is consistent with the following XRD results. The bondings of $CuFeMnO_4$-x NSAP were further investigated and confirmed by FT-IR spectra (Figure S1). The phase compositions and crystal structures of $CuFeMnO_4$-x were investigated with XRD measurements as shown in Figure S2. These diffraction peaks (marked with ∇) at 2θ = 18.2, 30.1, 35.6, 43.0, 57.0, 62.5, and 73.8° are ascribed to the (111), (220), (311), (400), (511), (440), and (533) reflections of cubic $CuFeMnO_4$. As-synthesized $CuFeMnO_4$ nanospheres are made of a cubic crystal system with a space group of $Fd\bar{3}m$, which matches well with the reported XRD data JCPDS No. 20-0358.[27] In addition, the diffraction peaks (marked with *) at 2θ = 43.3, 50.4, and 74.1° are ascribed to the (111), (200), and (220) reflections of cubic phase Cu (JCPDS No. 04-0836). On the basis of the XRD analyses, together with the SEM and TEM results, it is concluded that the Cu phase enters $CuFeMnO_4$ crystal lattice and thus leads to the formation of a whole piece of crystal but not segregated one. In our liquid-phase system, as a strong reducing agent, EG gives priority to reducing the Cu^{2+} to Cu because the reduction potential of Cu^{2+}/Cu (+0.337 V) is

DOI: 10.1021/acs.analchem.7b02476
Anal. Chem. 2017, 89, 10446−10453

Scheme 1. Schematic Representation of the Two-Stage Growth Mechanism of the $CuFeMnO_4$ NSAP

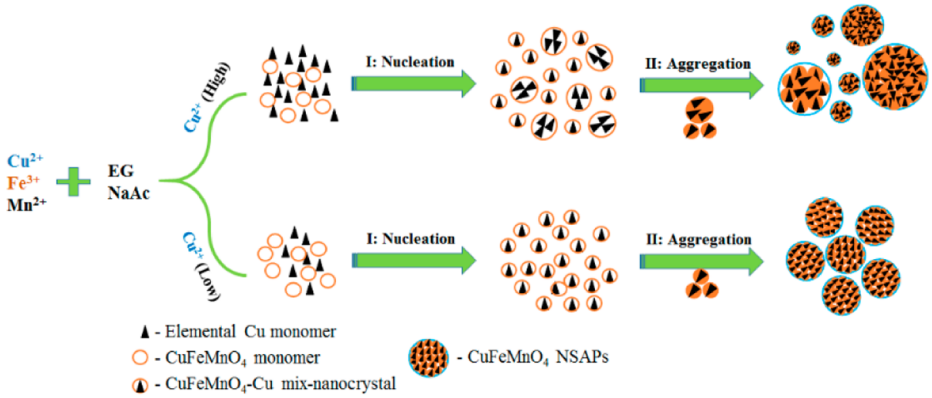

lower than that of Fe^{3+}/Fe^{2+} (+0.770 V). Therefore, this explains why the elemental Cu consists in $CuFeMnO_4$ crystal in the solvothermal synthetic process. This proposal is also supported by the presence of elemental Cu in $CuFe_2O_4$ particles synthesized with the same method.[34−37]

The magnetic properties of the prepared $CuFeMnO_4$-*x* affinity probes were measured by magnetometry at 300 K using a superconducting quantum interference device (SQUID). Figure S3 shows the hysteresis loops of them, and it is apparent that they possess superparamagnetic properties. The maximum saturation magnetization (M_s) values were measured to 42.6, 56.4, and 69.6 emu/g for $CuFeMnO_4$-01, $CuFeMnO_4$-02, and $CuFeMnO_4$-03, respectively. Consequently, such high magnetic saturation values impart $CuFeMnO_4$-*x* NSAP to the separation of target analytes by means of fast and convenient magnetic separation. It was observed that the M_s values of $CuFeMnO_4$-01 and $CuFeMnO_4$-02 were significantly lower than that of $CuFeMnO_4$-03 NSAP. On the basis of the above results, there is reason to suppose that the M_s values of $CuFeMnO_4$-*x* are dependent on the Cu content entering the $CuFeMnO_4$ crystal lattice, that is, the higher the Cu content, the weaker the magnetic property.

All in all, considering the particle size, uniformity, monodispersity, and M_s value, $CuFeMnO_4$-03 was chosen as the representative affinity material for further application. Therefore, unless otherwise specified, the name of the affinity nanosphere was expressed directly as $CuFeMnO_4$ NSAP, rather than through the serial number to distinguish the three nanospheres of different Cu contents.

Possible Formation Mechanism of $CuFeMnO_4$ NSAP. Solvothermal synthesis is an important technology for the preparation of nanostructures under the isobaric and low temperature. During their formation in the liquid-phase process, the as-prepared nanostructures are well-crystallized and controllable for particle sizes. Therefore, the solvothermal method is widely applied to nanostructure preparation.[38−40] In the present work, we reported that these monodisperse nanospherical $CuFeMnO_4$ NSAP was synthesized via a facile solvothermal reaction. The different concentration of precursors (Fe^{3+}, Cu^{2+}, and Mn^{2+}) can be used as the additional means to control and adjust the morphology and particle size. EG, as a strong reducing agent, can reduce the high-valent metal cations to low-valent ones or elemental metal under the auxiliary agent of sodium acetate (NaAc). A possible two-stage growth mechanism of $CuFeMnO_4$ NSAP is illustrated as shown in Scheme 1, including the primary nucleation of nanocrystals and the secondary aggregation. The details of the proposed mechanism with corresponding reaction equations were elucidated in PART 1 in Supporting Information.

Highly Specific Enrichment of Low-Abundance Peptides from Different Samples. In general, the functionalized *n*-alkyl chains are applied to capture hydrophobic peptides due to hydrophobic interaction,[41−43] while the immobilized or functionalized metal ions can simultaneously capture hydrophilic and hydrophobic peptides through their affinity to carboxyl and amino groups.[44−46] Among these metal ions, Cu^{2+} ions, which have strong and specific affinity toward peptides, can capture amino acid chains of the peptides via coordination bonds.[47] In our work, the surfaces of as-prepared $CuFeMnO_4$ NSAP are rich in metal ions (Cu^{2+}, Fe^{3+}, and Mn^{2+}), and thus, they have potential for applications that capture low-abundance peptides.

Model Sample (BSA Tryptic Digest (10 nM)). To inspect the possibility of the $CuFeMnO_4$ NSAP for enrichment of low-abundance peptides, we employed a 10 nM BSA tryptic digest as a model sample. For comparison, the commercial ZipTip C18 materials and Fe_3O_4 and $MnFe_2O_4$ nanoparticles were also adopted to enrich low-abundance peptides from a 10 nM BSA tryptic digest. The enrichment results were shown in the MALDI-TOF mass spectra (Figure 3), and the MALDI search results were provided in Appendixes S1−S5 in PART 5 in Supporting Information. Only seven peptides (marked with "∇", same below) were observed with low signal intensity and signal-to-noise ratio (S/N). However, after enrichment with the $CuFeMnO_4$ NSAP (100 μg), 17 peptides derived from the BSA tryptic digest can be detected with the increased MS intensity and S/N ratio. For example, the ALBU_BOVIN was successfully identified with a score of 120 and a protein sequence coverage ratio of 28%. In contrast, 14 peptides (Score: 91, sequence coverage: 24%), 13 peptides (Score: 90, sequence coverage: 19%), and 9 peptides (score: 68, sequence coverage: 15%) were detected, respectively, after being treated with $MnFeO_4$, Fe_3O_4, and ZipTip C18. The detailed information on their amino acid sequence is listed in Table S1. Compared with the ZipTip C18 materials, Fe_3O_4 and $MnFe_2O_4$ nanoparticles, $CuFeMnO_4$ NSAP exhibited intense binding affinity toward peptides due to metal ions, Fe^{3+}, Mn^{2+}, and Cu^{2+}, decorated on the surface of the magnetic nanospheres. Especially, a Cu^{2+}-rich surface has the potential for a strong coordination to the carboxyl and amine groups of peptides. Through analysis of the isoelectric point (pI) and the grand average hydrophobicity (GRAVY) values of the amino acid sequences, we can obtain their information on the acid−base property, hydrophilicity and hydrophobicity, respectively.

DOI: 10.1021/acs.analchem.7b02476
Anal. Chem. 2017, 89, 10446−10453

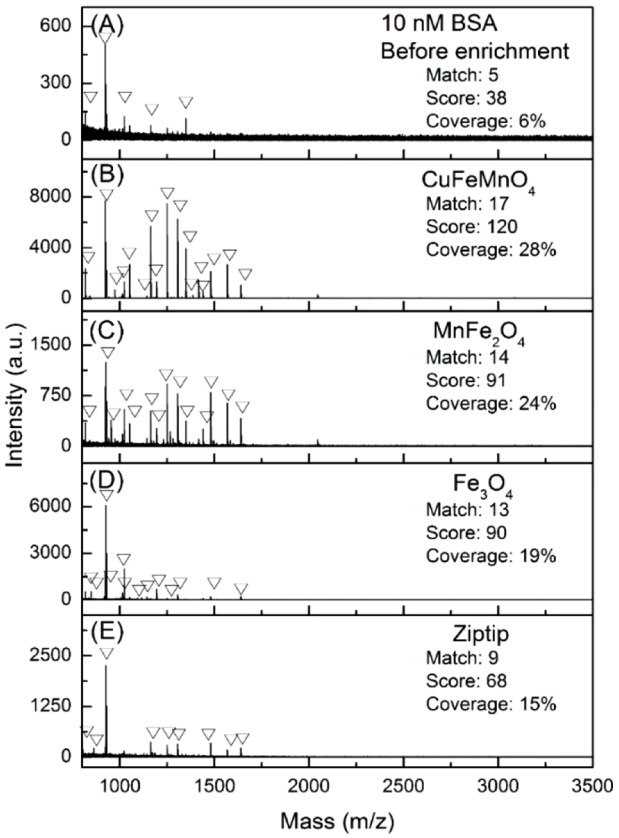

Figure 3. MALDI-TOF MS spectra of BSA tryptic digest (10 nM) without treatment (A), after treatment with $CuFeMnO_4$ NSAP (B), $MnFeO_4$ (C), Fe_3O_4 (D), and ZipTip C18 (E). "∇" indicates low-abundance peptides.

From the pI values of peptides obtained by treatment with $CuFeMnO_4$ NSAP, it can be seen that the distribution of pI was from 4.53 to 8.75. Fourteen acidic peptides accounted for 82.4% among them. In addition, the proportion of 11 hydrophilic peptides was 64.7% of the analysis of GRAVY value. Furthermore, we analyzed five high-intensity peptides (S/N > 1000) (red font in Table S1), and found that all of which were acidic peptides. Therefore, the above-mentioned results implied that the NSAP has a slight tendency to the hydrophilic and acidic peptides in the BSA tryptic digest based on synergistic action of the electrostatic interaction, and chelating or coordination of the metal ions with the carboxyl and/or the amine groups of peptides.

Practical Samples (2000-Fold Dilution of Human Saliva and Human Serum). Endogenous peptidome profiling of human saliva and human serum will provide important information for clinical diagnostics and prognosis of human disease. Human saliva/serum contain many informative proteins that can be used for the detection of diseases.[48−52] In this present study, to investigate practical application potential of $CuFeMnO_4$ NSAP, human saliva, and human serum were chosen as real-world samples for enriching low-abundance peptides. For comparison, $MnFeO_4$ and Fe_3O_4 nanoparticles were also employed as the control materials to enrich low-abundance peptides from the 2000-fold dilution of human saliva and human serum due to their convenient and fast magnetic separation. However, considering inconvenient separation and the relatively weaker enrichment capability in the model sample, ZipTip C18 was no longer applied in further tests of actual biological samples in the following experiments. As shown in Figures S4 and S5, the results of the analysis are similar for human saliva and human serum samples. Only several peptides with poor MS intensity and low S/N ratio were detected before enrichment (Figures S4A and S5A), while tens of peptides with high S/N ratio were observed, and their peak intensity increased sharply after treatment with $CuFeMnO_4$ NSAP (Figures S4B and S5B), indicating that the NSAP can selectively enrich low-abundance peptides from complex biosamples. In addition, it was found that the enrichment effect of $CuFeMnO_4$ NSAP was superior to that of $MnFe_2O_4$ and Fe_3O_4 nanoparticles due to the Cu^{2+}-rich surface of the NSAP.

Highly Specific Enrichment of Phosphopeptides from Different Samples. Metal oxide affinity chromatography (MOAC) has been extensively used to selectively enrich phosphopeptides. Essentially, for some metal oxides, such as TiO_2, ZrO_2, and SnO_2, together with some spinels, such as Fe_3O_4, $NiZnFe_2O_4$, $MnFe_2O_4$, and so on,[53−57] their surfaces have an amphoteric property due to the valence unsaturation of metal ions or the defectiveness of oxygen atom. These metal oxides are Lewis acid at low pH, and Lewis base at high pH. Metal oxide type has a strong reversible binding force with phosphate molecules due to the amphoteric property of its surface, which can be used for enrichment of phosphopeptides.[58] As a kind of spinel-like ternary metal oxide, $CuFeMnO_4$ has the potential to be applied in phosphopeptides enrichment and analysis. This is likely due to its surface composed of affinity rich-metal ions (Fe^{3+} and Mn^{2+}) and defective oxygen atoms.[57]

Mixture of Standard α-/β-Casein Tryptic Digests. The optimal pH in the loading buffer was quite different depending on the material used for phosphopeptides capture. The concentration of TFA was often used for pH adjustment.[59] In order to optimize the extraction condition, magnetic $CuFeMnO_4$-03 nanospheres were first utilized to enrich phosphopeptides from the mixture of tryptic digests of α-/β-casein (mole ratio, 1:1) as the test sample in eight different loading buffers (ACN%: 50%, TFA%: 0%−5.0%) as shown in Figure S6. The mixtures of peptides contained bovine β-casein tryptic digest (10 pmol), which remained constant in all test samples; they were incubated with $CuFeMnO_4$-03 NSAP (100 μg), and the phosphopeptides were selectively enriched by magnetic separation. When the range of TFA concentration in loading buffer was from 0% to 0.1%, i.e. the solution pH range was from neutral to 2.0 ($ACN:H_2O$ = 1:1), the phosphopeptides ion peaks with low MS signal were observed, but some strong nonphosphopeptides ion peaks also were detected and dominated the whole MALDI-TOF MS spectrum. However, when the range of TFA concentration was 0.5%−5.0% (pH ≤ 1.4), all the obtained peaks were phosphopeptides without any other interference peaks. The aforementioned results fully revealed that the pH adaptability of loading buffer for $CuFeMnO_4$-03 is less than or equal to 1.4. This can be explained by whether the phosphate group and the carboxyl group are protonated. When the pH of loading buffer is about 1.0−1.5, the carboxyl group of peptides is fully protonated, which can improve the high selectivity to phosphopeptides enrichment and reduce nonspecific adsorption. Nevertheless, because the acid dissociation constant of phosphate is 2.1, the phosphate group of phosphopeptides together with some acidic amino acid residues (such as glutamic and aspartic acids) begin to undergo a deprotonation reaction (pH > 2), which leads to

DOI: 10.1021/acs.analchem.7b02476
Anal. Chem. 2017, 89, 10446−10453

nonspecific adsorption between part of the carboxyl group and the metal cation ions.

To examine the enrichment efficiency of the $CuFeMnO_4$-x to phosphopeptides, we still took advantage of the above-mentioned test sample solution as an analysis objective, and 50%ACN-5.0%TFA was chosen as the loading buffer. The enrichment performance was evaluated with MS signal intensity and the number of captured phosphopeptides. Seven phosphopeptides (marked with "*", same below) with low MS signal, which was suppressed intensely by nonphosphopeptides, were detected before enrichment in the spectrum (Figure 4A). However, after being enriched with $CuFeMnO_4$-x NSAP,

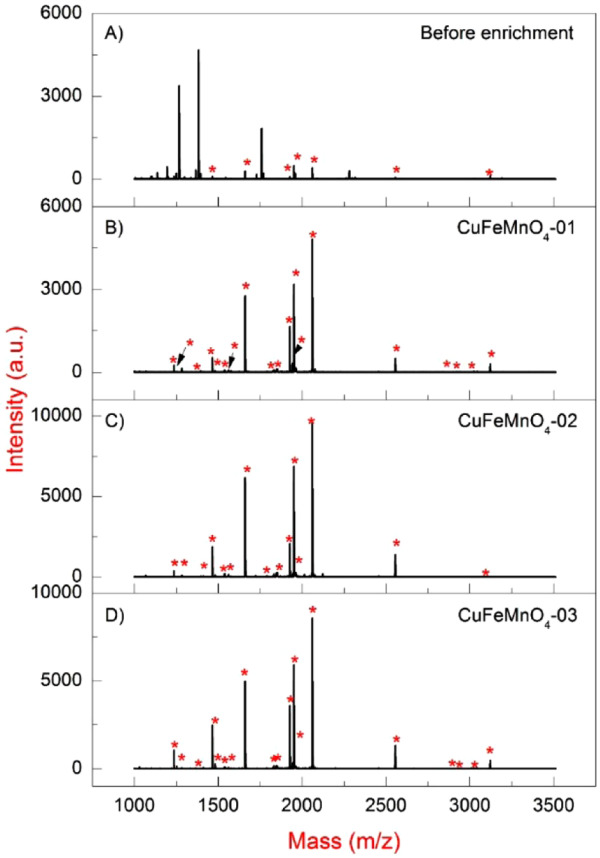

Figure 4. MALDI-TOF MS spectra of the mixture of bovine α-/β-casein digests (10 pmol, 1:1, v/v) before enrichment (A), treated with $CuFeMnO_4$-01 (B), $CuFeMnO_4$-02 (C), and $CuFeMnO_4$-03 (D) NSAP. "*" indicates phosphopeptides.

19 phosphopeptides with clean background can be observed and are free of the interference of nonphosphopeptides peaks. The corresponding peptide sequences of 19 phosphopeptide ions are listed in Table S2. In addition, the MS signals of these phosphopeptides increased significantly. Results showed that these three $CuFeMnO_4$ nanospheres have the same ability to selectively enrich phosphopeptides from the test sample (Figure 4B–D).

The detection limit for phosphopeptide enrichment by $CuFeMnO_4$ NSAP was evaluated. As shown in Figure S7A,B, the mixture of bovine α-/β-casein tryptic digests (1:1, v/v), with 100 fmol β-casein tryptic digest, results in three phosphopeptides that can be detected with $CuFeMnO_4$ NSAP. When the concentration was as low as 20 fmol, two phosphopeptides can still be observed, which demonstrates the high detection sensitivity of the affinity probe.

To assess the selectivity of the $CuFeMnO_4$ affinity probes for phosphopeptide enrichment, we applied them to enrich the phosphopeptides from a complex peptide mixture consisting of α-/β-casein and BSA (1:1:100, molar ratio) as shown in Figure S7C,D. Through direct spotting sample analysis, no phosphopeptide was detected from the peptide mixture due to the suppression effect and interference from the abundant nonphosphopeptides. However, after being treated with $CuFeMnO_4$ NSAP, 14 phosphopeptides can be clearly obtained with no other interference peaks in the mass spectrum (Figure S7D). On the basis of the above results, it further indicated that highly efficient capture and selective enrichment of phosphopeptides from complex peptides mixture were realized with $CuFeMnO_4$ NSAP treatment.

Practical Biological Samples (Nonfat Milk Tryptic Digest, Human Saliva, and Human Serum). To investigate practical application potential of $CuFeMnO_4$ NSAP, nonfat milk, human saliva, and human serum were chosen as real-world biological samples for phosphopeptides isolation as shown in Figure S8. For the nonfat milk tryptic digest, only two weak phosphopeptides peaks were observed in the direct analysis due to the nonphosphopeptides suppression effect and interference, as shown in the mass spectrum (Figure S8A). However, after selective capture using the NSAP, 10 phosphopeptides can be clearly detected in the mass spectrum and are free of the nonphosphopeptides interference (Figure S8B).

Human saliva and human serum containing various informative endogenous peptides including the phosphopeptides released by diseased tissue and these peptides have gained considerable interest for the disease biomarker discovery.[60,61] To further prove the practical application of the NSAP, we employed human saliva and human serum as biosamples for the selective enrichment of endogenous phosphopeptides. Through direct spotting sample analysis of the diluted human saliva, no phosphopeptide was detected owing to the nonphosphopeptides suppression effect (Figure S8C). In contrast, nine of endogenous phosphopeptides can be easily observed with a clean background in the mass spectrum (Figure S8D). In addition, for human serum sample, only two weak phosphopeptide peaks were detected before enrichment because of the suppression effect and interference from nonphosphopeptides, while four endogenous phosphopeptides with high MS signal derived from phosphorylated fibrinopeptide A can be identified in the mass spectrum and are free of the interference of nonphosphopeptide peaks after enrichment (Figure S8E,F). These identified endogenous phosphopeptides from human saliva and human serum are listed in Table S3.

A549 Cell Lysate Tryptic Digest. Encouraged by the emerging advantages of the $CuFeMnO_4$ NSAP toward phosphopeptides, we further applied the tryptic digests of a cell lysate as the real complex biosample because this type of sample is commonly investigated in phosphoproteomics analysis.[62−65] Figure S9A,C,E present the direct MALDI mass spectra of the tryptic digests of three A549 cell lysates (exposed to ZnO nanoparticle for 0, 9, and 24 h). There were a number of peaks appearing in the MALDI mass spectra, but no phosphopeptides were observed due to the serious suppression effect and interference of abundant nonphosphopeptides. Nevertheless, after being treated with the NSAP, there were some phosphopeptides visible in the mass spectra (Figure S9D,F) except for the mass spectrum (Figure S9B). The

DOI: 10.1021/acs.analchem.7b02476
Anal. Chem. 2017, 89, 10446−10453

identified amino acid sequences of phosphopeptides and their protein names are listed in Table S3. Taking the 9 h lysate extract (Figure S9D) as an example, the detailed MALDI mass spectra of phosphopeptides, including I (935−1030 Da), II (1250−1355 Da), and III (1550−1700 Da), are pointed out in Figure S9D-I, D-II, and D-III, respectively. These adjacent peaks represent the Na^+ adducted ion peaks (Δ22 Da), or oxidation on methionine ([Mo], Δ16 Da), or deletion/truncation of N-terminal on glutamine (*Q, Δ17 Da) for corresponding phosphopeptides. Theoretically, all these three cell lysates should contain phosphopeptides. However, no peaks were detected in the 0 h lysate, while some phosphopeptides were detected in the 9 and 24 h lysates. The results indicated that the expression of some phosphoproteins/phosphopeptides upregulated after a certain duration of exposure to ZnO nanoparticles. A549 cells were stimulated by exogenous substances (ZnO nanoparticles), and the A549 cells will make the corresponding signal response. For example, actin, cytoplasmic 2, which is regulated protein in the process, participates in signal pathways for bacterial invasion of epithelial cells using Kyoto Encyclopedia of Genes and Genomes (KEGG) (Figure S10). Actin acts as an important role in the signal pathway not only in zipper model but also in trigger model.[66,67] Through the selective and effective enrichment of phosphopeptides for phosphoprotome analysis of cell lysate after exposure to exogenous stimuli, we have proposed an approach to get insight into the possible changes of phosphoproteins/phosphopeptides in signaling pathways.

CONCLUSIONS

In the present work, the facile solvothermal reaction was employed for the first time to prepare the multifunctional and monodisperse ternary metal oxide magnetic spinel ferrite ($CuFeMnO_4$ NSAP). The uniform size of the $CuFeMnO_4$ nanospheres can be controlled by the concentration of Cu^{2+} precursor. Additonally, their excellent magnetic responsiveness endowed them with convenient and rapid magnetic separation. Based on their potentialities of strong coordination to carboxyl and amine groups of peptides (Cu^{2+}/Fe^{3+}-rich) and of binding affinity to phosphate groups of phosphopeptides (Fe^{3+}/Mn^{2+}-rich), the nanostructured affinity probe can not only enrich low-abundance peptides under neutral conditions but also selectively capture and separate phosphopeptides under acid conditions from complex biomolecules (human saliva and human serum) for MALDI-TOF MS detection. Moreover, we applied the $CuFeMnO_4$ NSAP to selectively capture and isolate phosphopeptides from A549 cells exposed to ZnO nanoparticles for different time. Therefore, we developed a promising channel to investigate the differential expression of phosphoproteins in cellular signal transduction after exposure to exogenous stimuli.

ASSOCIATED CONTENT

Supporting Information

The Supporting Information is available free of charge on the ACS Publications website at DOI: 10.1021/acs.analchem.7b02476.

Supplementary experimental section; FT-IR spectra, XRD patterns, and hysteresis loops of $CuFeMnO_4$ NSAP characterization; Detailed elucidation for two-stage growth mechanism of $CuFeMnO_4$ NSAP; Performance of $CuFeMnO_4$ NSAP as well as other affinity probes in low-abundance peptides enrichment from human saliva and serum; Performance of $CuFeMnO_4$ NSAP in phosphopeptides isolation from standard phosphoproteins mixture, nonfat milk, and A549 cell lysates tryptic digests, and human saliva and serum; Comparison of $CuFeMnO_4$ NSAP with previously reported materials for the enrichment of low abundance peptides and/or phosphopeptides. Amino acid sequences of identified low abundant peptides from tryptic digests of 10 nM BSA, together with phosphopeptides from tryptic digests of α-/β-casein, nonfat milk, human saliva and serum, and A549 cell lysates treated with $CuFeMnO_4$ NSAP; MASCOT search results for 10 nM BSA tryptic digest before enrichment and after treated with $CuFeMnO_4$ NSAP, $MnFeO_4$, and Fe_3O_4 nanoparticles, as well as commercial ZipTip C18 materials (PDF)

Observed phosphopeptides from the lysates of A549 cells after exposure to ZnO nanoparticles for different time (0, 9, and 24 h) by iTRAQ experiment (XLS)

AUTHOR INFORMATION

Corresponding Author

*Tel.: +86 25 83686075. E-mail: hzlian@nju.edu.cn.

ORCID

Hong-Zhen Lian: 0000-0003-1942-9248

Notes

The authors declare no competing financial interest.

ACKNOWLEDGMENTS

This work was supported by the National Natural Science Foundation of China (91643105, 21577057, 21275069), and the Analysis & Test Fund of Nanjing University.

REFERENCES

(1) Uttley, L.; Whiteman, B. L.; Woods, H. B.; Harnan, S.; Philips, S. T.; Cree, I. A. *EBioMedicine* **2016**, *10*, 164−173.

(2) Wu, H. Z.; Ong, K. L.; Seeher, K.; Armstrong, N. J.; Thalamuthu, A.; Brodaty, H.; Sachdev, P.; Mather, K. *J. Alzheimer's Dis.* **2016**, *49*, 755−766.

(3) Morgenthaler, N. G. *Congestive Heart Failure* **2010**, *16*, S37−S44.

(4) Fraser, K. B.; Moehle, M. S.; Alcalay, R. N.; West, A. B. *Neurology* **2016**, *86*, 994−999.

(5) Lindert, U.; Cabral, W. A.; Ausavarat, S.; Tongkobpetch, S.; Ludin, K.; Barnes, A. M.; Yeetong, P.; Weis, M.; Krabichler, B.; Srichomthong, C.; Makareeva, E. N.; Janecke, A. R.; Leikin, S.; Röthlisberger, B.; Rohrbach, M.; Kennerknecht, I.; Eyre, D. R.; Suphapeetiporn, K.; Giunta, C.; Marini, J. C.; Shotelersuk, V. *Nat. Commun.* **2016**, *7*, 11920.

(6) Schiess, R.; Wollscheid, B.; Aebersold, R. *Mol. Oncol.* **2009**, *3*, 33−44.

(7) Vallant, R. M.; Szabo, Z.; Bachmann, S.; Bakry, R.; Najam-ul-Haq, M.; Rainer, M.; Heigl, N.; Petter, C.; Huck, C. W.; Bonn, G. K. *Anal. Chem.* **2007**, *79*, 8144−8153.

(8) Petricoin, E. F.; Belluco, C.; Araujo, R. P.; Liotta, L. A. *Nat. Rev. Cancer* **2006**, *6*, 961−967.

(9) Diamandis, E. P. *J. Proteome Res.* **2006**, *5*, 2079−2082.

(10) Zhang, Y.; Wang, X.; Shan, W.; Wu, B.; Fan, H.; Yu, X.; Tang, Y.; Yang, P. *Angew. Chem., Int. Ed.* **2005**, *44*, 615−617.

(11) Jia, W.; Chen, X.; Lu, H.; Yang, P. *Angew. Chem.* **2006**, *118*, 3423−3427.

(12) Long, X.-Y.; Zhang, Z.-J.; Li, J.-Y.; Sheng, D.; Lian, H.-Z. *Chem. Commun.* **2017**, *53*, 4620−4623.

(13) Samanta, A.; Ravoo, B. J. *Angew. Chem., Int. Ed.* **2014**, *53*, 12946−12950.

DOI: 10.1021/acs.analchem.7b02476
Anal. Chem. 2017, 89, 10446−10453

(14) Nilsson, J.; Rüetschi, U.; Halim, A.; Hesse, C.; Carlsohn, E.; Brinkmalm, G.; Larson, G. *Nat. Methods* **2009**, *6*, 809−811.
(15) Li, J.; Wang, J.; Ling, Y.; Chen, Z.; Gao, M.; Zhang, X.; Zhou, Y. *Chem. Commun.* **2017**, *53*, 4018−4021.
(16) Fischnaller, M.; Bakry, R.; Vallant, R. M.; Huber, L. A.; Bonn, G. *Anal. Chim. Acta* **2013**, *761*, 92−101.
(17) Xu, L.; Ma, W.; Shen, S.; Li, L.; Bai, Y.; Liu, H. *Chem. Commun.* **2016**, *52*, 1162−1165.
(18) Zhao, L.; Qin, H.; Hu, Z.; Zhang, Y.; Wu, R.; Zou, H. *Chem. Sci.* **2012**, *3*, 2828−2838.
(19) Cheng, G.; Wang, Z.-G.; Liu, Y.-L.; Zhang, J.-L.; Sun, D.-H.; Ni, J.-Z. *ACS Appl. Mater. Interfaces* **2013**, *5*, 3182−3190.
(20) Xu, Y.; Wu, Z.; Zhang, L.; Lu, H.; Yang, P.; Webley, P. A.; Zhao, D. *Anal. Chem.* **2009**, *81*, 503−508.
(21) Zhu, G.-T.; He, X.-M.; He, S.; Chen, X.; Zhu, S.-K.; Feng, Y.-Q. *ACS Appl. Mater. Interfaces* **2016**, *8*, 32182−32188.
(22) Chen, X.; Li, S.; Zhang, X.; Min, Q.; Zhu, J.-J. *Nanoscale* **2015**, *7*, 5815−5825.
(23) Yan, Y.; Sun, X.; Deng, C.; Li, Y.; Zhang, X. *Anal. Chem.* **2014**, *86*, 4327−4332.
(24) Long, X.-Y.; Song, Q.; Lian, H.-Z. *J. Mater. Chem. B* **2015**, *3*, 9330−9339.
(25) Cheng, G.; Wang, Z.-G.; Liu, Y.-L.; Zhang, J.-L.; Sun, D.-H.; Ni, J.-Z. *Chem. Commun.* **2012**, *48*, 10240−10242.
(26) Zhang, Y.; Li, L.; Ma, W.; Zhang, Y.; Yu, M.; Guo, J.; Lu, H.; Wang, C. *ACS Appl. Mater. Interfaces* **2013**, *5*, 614−621.
(27) Jogalekar, P. P.; Sinha, A. P. B. *Indian J. Pure Appl. Phys.* **1967**, *5*, 9−13.
(28) Bergstein, A. *Mater. Res. Bull.* **1969**, *4*, 391−392.
(29) Tanaka, Y.; Takeguchi, T.; Kikuchi, R.; Eguchi, K. *Appl. Catal., A* **2005**, *279*, 59−66.
(30) Fan, Y.; Siriwardane, R.; Tian, H. *Energy Fuels* **2015**, *29*, 6616−6624.
(31) Kaluza, L.; Surca-Vuk, A.; Orel, B.; Drazic, G.; Pelicon, P. *J. Sol-Gel Sci. Technol.* **2001**, *20*, 61−83.
(32) Kim, T. K.; VanSaders, B.; Caldwell, E.; Shin, S.; Liu, Z.; Jin, S.; Chen, R. *Sol. Energy* **2016**, *132*, 257−266.
(33) Zou, Z. C.; Yang, K. H.; Chen, Z. S. *Chem. Res. Appl.* **2013**, *25*, 1050−1054.
(34) Zhu, M. Y.; Meng, D. H.; Wang, C. J.; Diao, G. W. *ACS Appl. Mater. Interfaces* **2013**, *5*, 6030−6037.
(35) Solano, E.; Perez-Mirabet, L.; Martinez-Julian, F.; Guzmán, R.; Arbiol, J.; Puig, T.; Obradors, X.; Yañez, R.; Pomar, A.; Ricart, S.; Ros, J. *J. Nanopart. Res.* **2012**, *14*, 1034.
(36) Bao, N.; Shen, L.; Wang, Y.; Padhan, P.; Gupta, A. *J. Am. Chem. Soc.* **2007**, *129*, 12374−12375.
(37) Zheng, J.; Lin, Z.; Liu, W.; Wang, L.; Zhao, S.; Yang, H.; Zhang, L. *J. Mater. Chem. B* **2014**, *2*, 6207−6214.
(38) Zhao, P.; Wang, J.; Cheng, G.; Huang, K. *J. Phys. Chem. B* **2006**, *110*, 22400−22406.
(39) Rajamathi, M.; Seshadri, R. *Curr. Opin. Solid State Mater. Sci.* **2002**, *6*, 337−345.
(40) Seidlhofer, B.; Pienack, N.; Bensch, W. *Z. Naturforsch., B: J. Chem. Sci.* **2010**, *65*, 937−975.
(41) Chen, H.; Xu, X.; Yao, N.; Deng, C.; Yang, P.; Zhang, X. *Proteomics* **2008**, *8*, 2778−2784.
(42) Chen, H.; Deng, C.; Zhang, X. *Angew. Chem., Int. Ed.* **2010**, *49*, 607−611.
(43) Liu, Q.; Shi, J. B.; Cheng, M. T.; Li, G. L.; Cao, D.; Jiang, G. B. *Chem. Commun.* **2012**, *48*, 1874−1876.
(44) Song, Q.; Zhao, W.-J.; Yin, H.-X.; Lian, H.-Z. *RSC Adv.* **2015**, *5*, 63896−63902.
(45) Zhao, M.; Deng, C.; Zhang, X. *ACS Appl. Mater. Interfaces* **2013**, *5*, 13104−13112.
(46) Zhao, M.; Deng, C.; Zhang, X.; Yang, P. *Proteomics* **2013**, *13*, 3387−3392.
(47) Liu, S.; Chen, H.; Lu, X.; Deng, C.; Zhang, X.; Yang, P. *Angew. Chem., Int. Ed.* **2010**, *49*, 7557−7561.
(48) Hu, S.; Wang, J.; Meijer, J.; Ieong, S.; Xie, Y.; Yu, T.; Zhou, H.; Henry, S.; Vissink, A.; Pijpe, J.; Kallenberg, C.; Elashoff, D.; Loo, J. A.; Wong, D. T. *Arthritis Rheum.* **2007**, *56*, 3588−3600.
(49) Terracciano, R.; Preianò, M.; Palladino, G. P.; Carpagnano, G. E.; Barbaro, M. P. F.; Pelaia, G.; Savino, R.; Maselli, R. *Proteomics* **2011**, *11*, 3402−3414.
(50) Petricoin, E. F.; Belluco, C.; Araujo, R. P.; Liotta, L. A. *Nat. Rev. Cancer* **2006**, *6*, 961−967.
(51) Cho, W. C. S.; Yip, T. T. C.; Yip, C.; Yip, V.; Thulasiraman, V.; Ngan, R. K. C.; Yip, T.-T.; Lau, W.-H.; Au, J. S. K.; Law, S. C. K.; Cheng, W.-W.; Ma, V. W. S.; Lim, C. K. P. *Clin. Cancer Res.* **2004**, *10*, 43−52.
(52) Liotta, L. A.; Petricoin, E. F. *J. Clin. Invest.* **2006**, *116*, 26−30.
(53) Yan, J. Y.; Li, X. L.; Cheng, S. Y.; Ke, Y. X.; Liang, X. M. *Chem. Commun.* **2009**, *20*, 2929−2931.
(54) Ma, R. N.; Hu, J. J.; Cai, Z. W.; Ju, H. X. *Talanta* **2014**, *119*, 452−457.
(55) Long, X.-Y.; Li, J.-Y.; Sheng, D.; Lian, H.-Z. *RSC Adv.* **2016**, *6*, 96210−96222.
(56) Zhong, H. Y.; Xiao, X.; Zheng, S.; Zhang, W. Y.; Ding, M. G.; Jiang, H. Y.; Huang, L. L.; Kang, J. *Nat. Commun.* **2013**, *4*, 1656−1662.
(57) Long, X.-Y.; Li, J.-Y.; Sheng, D.; Lian, H.-Z. *Talanta* **2017**, *166*, 36−45.
(58) Leitner, A.; Sturm, M.; Lindner, W. *Anal. Chim. Acta* **2011**, *703*, 19−30.
(59) Qi, X.; Chen, L.; Zhang, C.; Xu, X.; Zhang, Y.; Bai, Y.; Liu, H. *ACS Appl. Mater. Interfaces* **2016**, *8*, 18675−18683.
(60) Sreebny, L. M. *Int. Dent. J.* **2000**, *50*, 140−161.
(61) Hanash, S. M.; Pitteri, S. J.; Faca, V. M. *Nature* **2008**, *452*, 571−579.
(62) Yu, G.; Xiao, C.-L.; Lu, C.-H.; Jia, H.-T.; Ge, F.; Wang, W.; Yin, X.-F.; Jia, H.-L.; He, J.-X.; He, Q.-Y. *Mol. BioSyst.* **2011**, *7*, 472−479.
(63) Sudhir, P.-R.; Hsu, C.-L.; Wang, M.-J.; Wang, Y.-T.; Chen, Y.-J.; Sung, T.-Y.; Hsu, W.-L.; Yang, U.-C.; Chen, J.-Y. *PLoS One* **2011**, *6*, e20199.
(64) Dapat, C.; Saito, R.; Suzuki, H.; Horigome, T. *Virus Res.* **2014**, *179*, 53−63.
(65) Kim, J.-Y.; Welsh, E. A.; Oguz, U.; Fang, B.; Bai, Y.; Kinose, F.; Bronk, C.; Remsing Rix, L. L.; Beg, A. A.; Rix, U.; Eschrich, S. A.; Koomen, J. M.; Haura, E. B. *Proc. Natl. Acad. Sci. U. S. A.* **2013**, *110*, 12414−12419.
(66) Guerra, C. R.; Seabra, S. H.; de Souza, W.; Rozental, S. *PLoS One* **2014**, *9*, e89250.
(67) Eierhoff, T.; Bastian, B.; Thuenauer, R.; Madl, J.; Audfray, A.; Aigal, S.; Juillot, S.; Rydell, G. E.; Müller, S.; de Bentzmann, S.; Imberty, A.; Fleck, C.; Römer, W. *Proc. Natl. Acad. Sci. U. S. A.* **2014**, *111*, 12895−12900.

DOI: 10.1021/acs.analchem.7b02476
Anal. Chem. 2017, 89, 10446−10453